On the Mechanical Characterization of Human Humerus using Multi-scale Continuum Finite Element Model

F. Vandenbulcke[1], J. Rahmoun[1], H. Morvan[1], H. Naceur[1], P. Drazetic[1], C. Fontaine[2], R. Bry[2]

Abstract This paper is devoted to the characterization of human humerus behavior using a multi-scale approach for the estimation of the ultimate impact load. First, we present the experimental tests on human humeral bone in order to identify and quantitatively assess the mechanical properties. Then, we propose a micromechanical modeling of the elastic anisotropic properties of the humerus based on the coupling between the Mori-Tanaka homogenization scheme and a hex-shell Finite Element model. The obtained micromechanical model is implemented via a UMAT routine within the explicit dynamic code LS-DYNA©. The obtained numerical results show globally good agreement when compared to the experimental measurements.

Keywords Humerus human bone, elastic homogenization, micromechanical modeling, FEM.

I. INTRODUCTION

Measurement of density, geometric properties and mechanical strength are important features when evaluating and describing bone tissues. As one of the major functions of bone is to provide structural support for the musculoskeletal system, a correct assessment of its mechanical strength is desirable in most experiments that might alter the biological mechanisms regulating bone tissue [8]. More particularly, mechanical properties of the humerus bone are of interest. A good understanding of bone mechanical behavior allows to evaluate the fracture risk and to quantify an appropriate response for treatment [11]. This knowledge may also help for choosing optimal fixation techniques and locations for prosthetic components and then suggest optimized surgical procedures to preserve stronger bone to enhance implant fixation. However, in the literature most of research studies have focused on femoral and tibia bone [12] and only few investigations have been conducted on the humeral and radial bones [6, 8, 11].

The aim of the present work is to propose a consistent multi-scale approach for the accurate characterization and modeling of mechanical human humerus material parameters under impact. The present micromechanical model [10] is based on the coupling between the Mori-Tanaka homogenization scheme [9] for the estimation of elastic properties of humeral bone using the Eshelby inclusion problem [3], and a 3D hexahedral FE model [4] at the macro-level for the prediction of the global humerus response. The proposed procedure consists in two stages: at first, we perform a local identification of the bone matrix material parameters through the use of mechanical tension/compression testing on rectangular specimens extracted directly from the humerus. Once the bone matrix material parameters (Young's modulus, void aspect ratio, porosity) are identified, a homogenized scheme is used within a finite element model to identify the macroscopic anisotropic material parameters in longitudinal and transverse fiber directions. These macroscopic anisotropic material parameters are then used, as material data, to evaluate the global response of a humerus under impact.

The paper is structured as follows: the introduction is given in section 1. Section 2 presents the experimental campaign on local specimens and the impact of the humerus using the drop tower device, followed with a presentation of the main aspects of the multi-scale continuum finite element model. Results of humerus material parameters identification and further results of the impact test are given in section 3. In section 4 we discuss the relevance of the obtained results and assessments to be provided for further developments. Finally some conclusions are drawn in section 5 on the basis of this first investigation on the mechanical

[1] Laboratory LAMIH, University of Valenciennes, 59313 Valenciennes Cedex 9, France
[2] Laboratory of Anatomy, University of Lille 2, 59000 Lille, France
* Correspondence: Pr. H. Naceur, e-mail: hakim.naceur@univ-valenciennes.fr, Phone: +33.327.511.412

characterization of human humerus behavior.

II. METHODS

Six full humerus bones are obtained from three human cadavers, with an average age of 63 years. The humerus specimens were supplied by the Laboratory of Anatomy of Lille University in accordance with French regulations. Each specimen has been submitted to a virological and serological analysis and did not exhibit any bone disease on radiographic examination. All specimens were embalmed and stored at 4°C until the beginning of the experiments.

Scans of each specimen were performed using a 3D scanner VIVID 910 KONICA MINOLTA. These acquisitions are performed prior to preparing the humerus for the mechanical testing and the extraction of the precise boundary conditions. Digital geometry data are saved in the STL standard format and sent to a CAD workstation. After segmenting the individual bone regions, we obtained the full 3D digital models of the humerus by performing 3D surface generation of the bone cortex.

Mechanical experiments on local humerus specimens

In order to perform the local identification of the humeral bone material parameters, a first experimental campaign is carried out using several uniaxial tension/compression tests at room temperature (20°C) on a Dynamic Mechanical Analyzer (DMA) device (Figure 1c) available at laboratory LAMIH.

Five small specimens (H1-H5) are extracted from the same humerus (the right side of one corpse) as shown in Figure 1. The bone samples are obtained by carefully sectioning the lateral cortices of the mid-diaphysis of the humerus. The prismatic-shaped specimens have an average size of $50 \times 10 \times 3.5mm$ (Figure 1a).

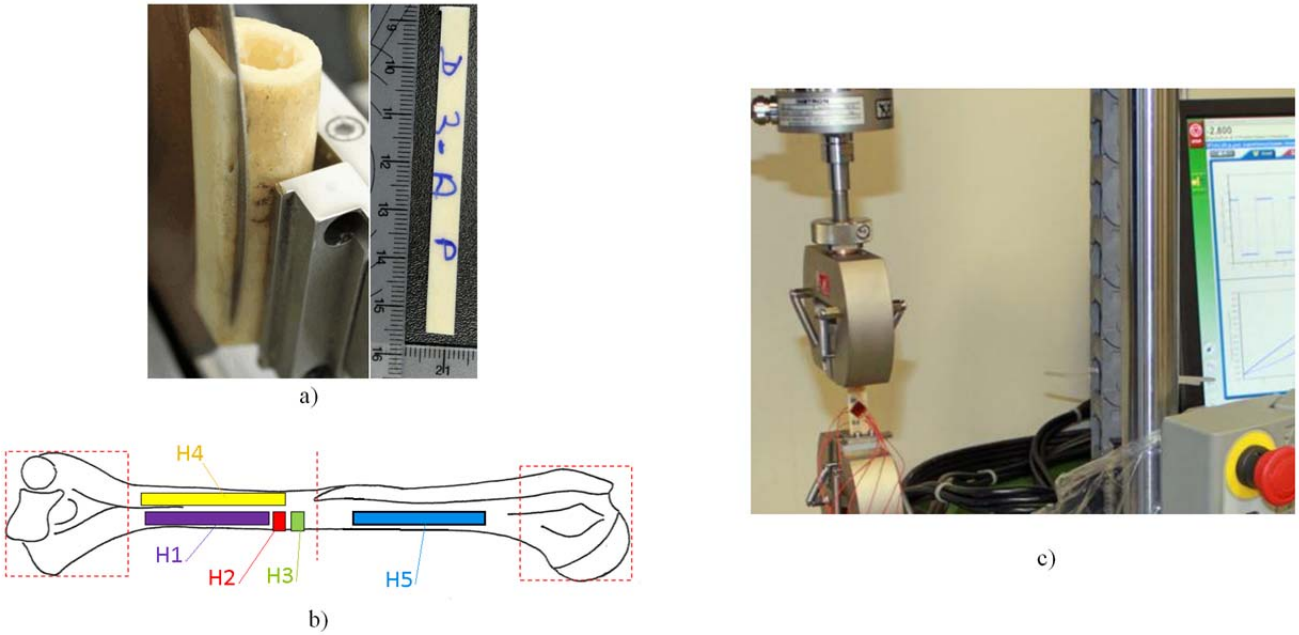

Fig. 1. Mechanical experiments on local specimens using the DMA device

In order to study the repeatability and also to avoid measurement errors, several tension/compression tests are carried out for each specimen. For the three longitudinal specimens, namely H1, H4 and H5 (see Figure 1 *b*), 19, 10 and 5 cyclic tension/compression tests have been undertaken respectively. For the two transverse specimens, namely H2 and H3, 7 and 5 cyclic tension/compression tests are performed using the DMA device as shown in Figure 1c.

Each specimen is instrumented using five gauges for strain measurement. Two strain gauges are fixed on the top layer for the longitudinal and the transverse strain measurement and three gauges are fixed on the bottom surface of the specimen to measure the shearing and the longitudinal strains. Each specimen is loaded up to 0.2% deformation with several velocities covering a range of 1-10 mm/mn. Each test provides a load/displacement and stress/strain curves, characteristic of the local mechanical behavior of the specimen.

Experimental study of low velocity impact on a human humerus

The second stage of the proposed procedure consists in performing a global experimental study of low velocity impact on a full human humerus using a drop tower, in order to validate the numerical model. For this purpose, the humerus of the left side of the same corpse is used. Two prismatic brackets (Figure 2*a*) in which the humerus is positioned are placed on a straight support to ensure their parallelism. One of the brackets is fixed, while the other is free to slide in order to be adapted to the length of the bone. Four positioning screws (Figure 2*a*) are used to help maintain the head and the lateral epicondyle of the humerus in a fixed position.
The system humerus-brackets, is first positioned vertically and a FASTCAST© Polyurethane resin (type F14-F15 from Axson Company) is poured into the lower bracket. Three hours later (resin drying time), the humerus-brackets system is returned and the same operation is done for the second bracket. The impact on the humerus is chosen to hit in the middle of the diaphysis. The bone is instrumented using 5 strain gauges and 3 patterns as shown in Figure 2a.

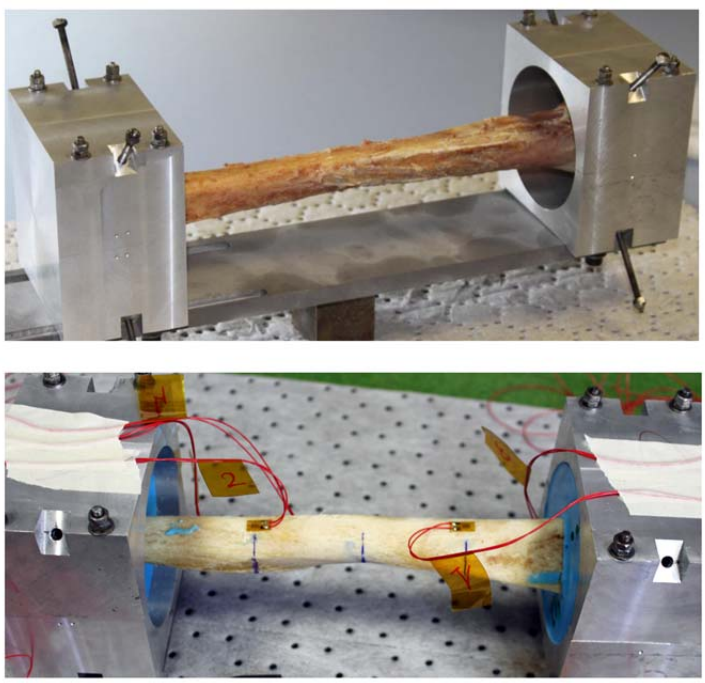

a) Humerus instrumentation

b) Drop tower device

Fig. 2. Experimental study of low velocity impact on a human humerus

After instrumentation the humerus is scanned in order to obtain the exact physical boundary conditions of the system humerus-brackets as well as the precise locations of the gauges to perform comparison with the finite element model.
The impact is performed experimentally with a projectile of 6626 g mass, with an initial velocity of 1.79 m/s. The total impact energy of the present impact test is 10 J which was shown from previous research works [2], to be necessary to reach the human humerus ultimate strength. The humerus instrumentation together with high speed camera (3000 fps) provides a precise recording of the evolution of the impact load as well as the displacements/strain curves in function of time.

Theoretical description of multi-scale continuum finite element model

a) Theoretical assumptions of the micromechanical model

In the present study, the human humeral bone is considered as a multiscale heterogeneous porous material with a matrix phase weakened by micro-pores and which exhibits transversely isotropic symmetry. The representative volume element (RVE) of bone is composed of an isotropic elastic solid matrix with stiffness tensor $C^{(m)}$ and a random distribution of ellipsoidal shaped voids made up of phases r ($r=1,...,N$) with the $C^{(r)}$ tensor.

According to the isotropy assumption of the solid matrix, the stiffness tensor $C^{(m)}$, reads $C^{(m)} = 3\kappa^{(m)}J + 2\mu^{(m)}K$, where $\kappa^{(m)}$ and $\mu^{(m)}$ represent the bulk and shear moduli of the matrix, respectively and where the fourth order tensors J and K are the isotropic fourth order tensor projectors having minor and major symmetries. The inclusions of the phase r are taken to be identical in shape and orientation with normal $\underline{n}$, radius a and the average half-opening c. Let E be the uniform macroscopic strain field prescribed on the boundary of the RVE. The corresponding displacement $u(x)$ boundary condition reads:

$$u(x) = E.x \quad (\forall x \varepsilon \partial\Omega) \tag{1}$$

Assuming now a linear elastic behavior for each phase within the RVE, the constitutive relation is given in the form $\sigma(x) = C(x) : \varepsilon(x), \ \forall\, x\ \varepsilon\ \Omega$. Accordingly, a fourth-order concentration tensor $A(x)$, relating the microscopic strain $\varepsilon(x)$ to the macroscopic strain E, is introduced:

$$\varepsilon(x) = A(x) : E \tag{2}$$

Taking the average of the microscopic stress $\sigma(x)$ and using (2), the macroscopic elastic behavior of material can be expressed in the form $\Sigma = C^{hom} : E$, with

$$C^{hom} = < C(x) : A(x) >_{\Omega} \tag{3}$$

Based on matrix-inclusion problems [3] and the Mori-Tanaka scheme [9] which commonly deals with inclusions interaction in composite materials, we assume a constant localization tensor by phase. Then, by using the identity $< A >_{\Omega} = I$ in (3), an estimate for the homogenized elastic stiffness tensor of the heterogeneous material reads as [10]:

$$C^{hom} = C^{(m)} + \sum_{r=1}^{N} f^{(r)} (C^{(r)} - C^{(m)}) : A_w^{(r)} : (f^{(m)} I + \sum_{s=1}^{N} f^{(s)} A_w^{(s)})^{-1} \tag{4}$$

where $f^{(m)}$ and $f^{(r)}$ are, respectively, the volume fraction of matrix and inclusions and where the two sums are taken over all phases of the heterogeneous material in the RVE. $A_w^{(r)}$ denotes the strain concentration tensor associated with the rth phase family of inclusions of aspect ratio $w = \dfrac{c}{a}$, which writes:

$$A_w^{(r)} = [I + P_w^{(r)} : (C^{(r)} - C^{(m)})]^{-1} \tag{5}$$

and $P_w^{(r)}$ is the Hill tensor [5]. This tensor depends on the shape and orientation of the rth family of inclusions $C^{(r)}$ (considered here as spheroid) and the elastic stiffness of the reference medium $C^{(m)}$. This tensor reads is defined by (see [5]):

$$P_{ijpq}^{(r)} = \frac{a^2 c}{4\pi} \int_{|\xi|=1} \frac{\xi_i \left[K^{(m)}\left(\underline{\xi}\right)\right]_{jp}^{-1} \xi_q \Big|_{(ij)(pq)}}{\left(\sqrt{a^2(\xi_1^2+\xi_2^2)+c^2\xi_3^2}\right)^3} dS(\underline{\xi}) \tag{5b}$$

for which the integration is on the unit sphere centered at the origin of space (ξ_1, ξ_2, ξ_3), defined by $|\xi| = 1$. $K_{ip}^{(m)}\left(\underline{\xi}\right) = C_{ijpq}^{(m)} \xi_j \xi_q$ is called the acoustic tensor. The notation $|_{(ij)(pq)}$ indicates the symmetrization with respect to the couples (i,j) and (p,q). Let us notice that, for the porous humeral bone, the effective stiffness tensor (4) reduces to:

$$C^{hom} = C^{(m)} + f^{(p)} (C^{(p)} - C^{(m)}) : A_w^{(p)} : (f^{(m)} I + f^{(p)} A_w^{(p)})^{-1} \tag{6}$$

Where $f^{(p)}$ is the porosity and where $C^{(p)}$ is the stiffness tensor of the porous humeral bone.
Finally, as in the previous work [10], the formalism of stiffness tensor (6) is coupled with experimental measurements of architectural anisotropy obtained from X-ray micro tomography and the Mean Intercept Length (MIL) method, which will, in turn, be used to calculate the porosity.

b) Theoretical review of the macroscopic eight-node Hex-Shell FE model

In this section, the formulation of the eight-node Hex-Shell element is briefly recalled. With respect to nodal designation (see Figure 3a), the coordinate vector $\mathbf{X}$ and displacement vector $\mathbf{U}_q$ of the element are [4]

$$\mathbf{X}_q(\xi,\eta,\zeta) = \mathbf{X}_0(\xi,\eta) + \zeta \mathbf{X}_n(\xi,\eta) = \sum_{i=1}^{4} N_i(\xi,\eta) \left(\frac{1-\zeta}{2} \mathbf{X}_i^- + \frac{1+\zeta}{2} \mathbf{X}_i^+ \right) \tag{7}$$

$$\mathbf{U}_q(\xi,\eta,\zeta)=\mathbf{U}_0(\xi,\eta)+\zeta\mathbf{U}_n(\xi,\eta)c=\sum_{i=1}^{4}N_i(\xi,\eta)\left(\frac{1-\zeta}{2}\mathbf{U}_i^- +\frac{1+\zeta}{2}\mathbf{U}_i^+\right) \tag{8}$$

where N_i are the two-dimensional eight-node Lagrangian interpolation functions, $\mathbf{X}_i^-$, $\mathbf{U}_i^-$ and $\mathbf{X}_i^+$, $\mathbf{U}_i^+$ are respectively, the coordinate and displacement vectors of the i^{th} node on the bottom and top shell surfaces (Figure 3a).

The infinitesimal covariant element strains with respect to the parametric coordinates are given by

$$\varepsilon_{\xi\xi}=\mathbf{X}_{,\xi}^T\,\mathbf{U}_{,\xi};\ \varepsilon_{\eta\eta}=\mathbf{X}_{,\eta}^T\,\mathbf{U}_{,\eta};\ \gamma_{\xi\eta}=\mathbf{X}_{,\xi}^T\,\mathbf{U}_{,\eta}+\mathbf{X}_{,\eta}^T\,\mathbf{U}_{,\xi} \tag{9}$$

$$\varepsilon_{\zeta\zeta}=\mathbf{X}_{,\zeta}^T\,\mathbf{U}_{,\zeta};\ \gamma_{\xi\zeta}=\mathbf{X}_{,\xi}^T\,\mathbf{U}_{,\zeta}+\mathbf{X}_{,\zeta}^T\,\mathbf{U}_{,\xi};\ \gamma_{\eta\zeta}=\mathbf{X}_{,\eta}^T\,\mathbf{U}_{,\zeta}+\mathbf{X}_{,\zeta}^T\,\mathbf{U}_{,\eta} \tag{10}$$

The constitutive relation of laminated composites can be described by using an orthotropic material law. For that purpose, we express the components of the tangent elastic moduli tensor relative to the fiber reference axis $\{a_1;a_2;a_3\}$ of a lamina.

$$C=\begin{bmatrix} C^{1111} & C^{1112} & 0 & C^{1113} & 0 & 0\\ C^{1122} & C^{2222} & 0 & C^{2223} & 0 & 0\\ 0 & 0 & C^{1212} & 0 & 0 & 0\\ C^{1133} & C^{2233} & 0 & C^{3333} & 0 & 0\\ 0 & 0 & 0 & 0 & C^{1313} & 0\\ 0 & 0 & 0 & 0 & 0 & C^{2323} \end{bmatrix} \tag{11}$$

where the components C^{ijkl} take the following expressions:

$$C^{1111}=E_1(1-\upsilon_{23}\upsilon_{32})/K;\quad C^{1122}=E_1(\upsilon_{21}+\upsilon_{23})/K;\quad C^{2222}=E_2(1-\upsilon_{13}\upsilon_{31})/K$$
$$C^{1113}=E_1(\upsilon_{31}+\upsilon_{21}\upsilon_{32})/K;\quad C^{2223}=E_2(\upsilon_{32}+\upsilon_{12}\upsilon_{31})/K;\quad C^{3333}=E_3(1-\upsilon_{12}\upsilon_{21})/K$$
$$C^{1212}=G_{12};\quad C^{1313}=G_{13};\quad C^{2323}=G_{23}$$
$$K=1-\upsilon_{12}\upsilon_{21}-\upsilon_{13}\upsilon_{31}-\upsilon_{23}\upsilon_{32}-2\upsilon_{12}\upsilon_{23}\upsilon_{31};\quad \nu_{ij}E_j=\nu_{ji}E_i$$

for ($i,j=1,2,3$ with $i\neq j$) and E_1, E_2, E_3 are the Young's moduli in the principal material directions $\{a_1;a_2;a_3\}$, respectively, and ν_{ij} and G_{ij} the Poisson's ratio and the shear modulus respectively.

Since matrix C is associated with the principal material directions, we need to transform it from the lamina coordinate axes $\{a_1;a_2;a_3\}$ to the global Cartesian coordinate axes $\{e_1;e_2;e_3\}$. With θ being the fiber orientation angle relative to the global Cartesian system, the relationship between the lamina coordinate system and the global Cartesian coordinate system is given by

$$a_1=\cos\theta\,e_1+\sin\theta\,e_2,\quad a_2=-\sin\theta\,e_1+\cos\theta\,e_2,\quad a_3=e_3 \tag{12}$$

The final constitutive tensor C can be expressed in the convective basis

$$\tilde{C}=T_G^T\,C\,T_G \tag{13}$$

In order to deal with the several lockings, one needs to split the expression of the virtual internal work into three contributions, by uncoupling the membrane/bending, thickness and transverse shear [4].

$$W_{int}=W_{int}^{mf}+W_{int}^{ez}+W_{int}^{c} \tag{14}$$

with:

$$W_{int}^{mf}=\int_V \delta\varepsilon_s{}^T\,\tilde{C}_1\,\varepsilon_s\,dv=\delta\mathbf{u}_n{}^T\,\mathbf{R}_{mf};\quad \mathbf{R}_{mf}=\int_v B_{mf}^T\,\sigma_{mf}\,dv \tag{15}$$

$$W_{int}^{ez}=\int_V \delta\varepsilon_z{}^T\,\tilde{C}_2\,\varepsilon_z\,dv=\delta\mathbf{u}_n{}^T\,\mathbf{R}_{ez};\quad \mathbf{R}_{ez}=\int_v B_z^T\,\sigma_z\,dv \tag{16}$$

$$W_{int}^{c}=\int_V \delta\gamma_s{}^T\,\tilde{C}_3\,\gamma_s\,dv=\delta\mathbf{u}_n{}^T\,\mathbf{R}_c;\quad \mathbf{R}_c=\int_v B_c^T\,\sigma_c\,dv \tag{17}$$

and $\varepsilon_{\mathbf{s}}{}^T=<\varepsilon_{xx}\quad\varepsilon_{yy}\quad\gamma_{xy}>$, $\varepsilon_z{}^T=<\varepsilon_{xx}\quad\varepsilon_{yy}\quad\varepsilon_{zz}>$, $\gamma_s{}^T=<\gamma_{xz}\quad\gamma_{yz}>$

A Hex-Shell element formulated using equations (15-17) with standard integration based on a $2\times2\times2$ Gauss schema will fail because of numerous locking phenomena. As already mentioned in previous works ([4]), shear locking is resolved using the Assumed Natural Strain (ANS) method, in which the natural shear strains are sampled and then interpolated at some discrete element points.
Similar to shear locking, trapezoidal and volumetric lockings occur when lower order elements such as eight-node hexahedral elements are used to model curved shells. In order to overcome these lockings, the Enhanced Assumed Strains (EAS) method is used where a linear distribution of the normal strain in thickness direction must be introduced to enhance the thickness strain field by adding a 7^{th} internal variable α which will be eliminated using a special condensation technique at the element level.

$$\tilde{\varepsilon}_z^{EAS} = \varepsilon_z^{ANS} + \alpha\,\zeta\,\mathbf{e}_3 \tag{18}$$

Finally the internal force vector is obtained using the modified strain fields by:

$$\mathbf{R} = \mathbf{R}_{mf} + \mathbf{R}_{ez}^{ANS} + \mathbf{R}_{c}^{EAS} \tag{19}$$

Numerical identification of the matrix material parameters

Based on the obtained experimental results, a numerical procedure for the identification of the humerus matrix material parameters has been carried out using our numerical model implemented within a UMAT in LS-DYNA© code [7]. A small prismatic-shaped specimen FE model of $50\times10\times3.5mm$ is discretized using 500 Hex-Shell elements (Figure 3b).

a) Hex-Shell Finite Element Model. b) Specimen FEM mesh using only 500 elements.

Fig. 3. Hex-Shell Finite Element Modeling

The inverse identification is performed, by taking as a reference data the average experimental results obtained for all tested specimens namely $E_l = 21368.33MPa$ and $E_t = 12516MPa$. In this investigation the Poisson ratio is not studied and is supposed to be fixed equal to the average experimental one. Three identification parameters are chosen, the elastic modulus of the bone matrix E_m, the voids aspect ratio w and the porosity fraction f_p.

TABLE II
DESIGN VARIABLE PROPERTIES

	E_m (MPa)	w	f_p
Initial value	20000	1.	0.0
Lower bound	20000	1.	0.0
Upper bound	25000	10.	0.1

At the beginning a Design Of Experiments (DOE) is built up based on a Full Factorial algorithm. Eleven uniformly spaced levels were taken for all three parameters (Table II). The objective function to be minimized is based on least squares error between the experimental and numerical stress-strain curves. The DOE generated using the 3 parameters with 11 levels for each, gives a set of 1331 runs. A Response Surface Model (RSM) is then created using a polynomial basis vector of degree 1, where the Analysis of Variance gives a R^2 value of 0.99.

Numerical simulation of the human humerus impact

The final stage of the proposed mechanical characterization of human humerus using a multi-scale continuum FE model consists of a drop tower test. The aim of the impact test at low velocity is the validation of the proposed numerical model in the estimation of the ultimate impact load.

The first step in this phase is the reconstruction of the 3D geometry of the humerus starting from the digitalized STL inner and outer surfaces of the humerus. As shown in Figure 6a, the digitalized STL mesh is split into two different parts (inner and outer surfaces). Then each STL surface is partitioned along the transverse direction into 12 small parts (Figure 6a) using HyperMesh© software [1]. Then, the 12 small local surfaces are generated based on the edges which have been regenerated thanks to HyperMesh© CAD facilities.

Once the total inner and outer surfaces of the humerus are built up, a first mapped shell mesh is generated using only quadrilateral shell elements. Then a 3D mesh of the humerus volume is generated with 4320 hexahedra, thanks to the 3D meshing facilities available in HyperMesh© software (see Figure 6b).

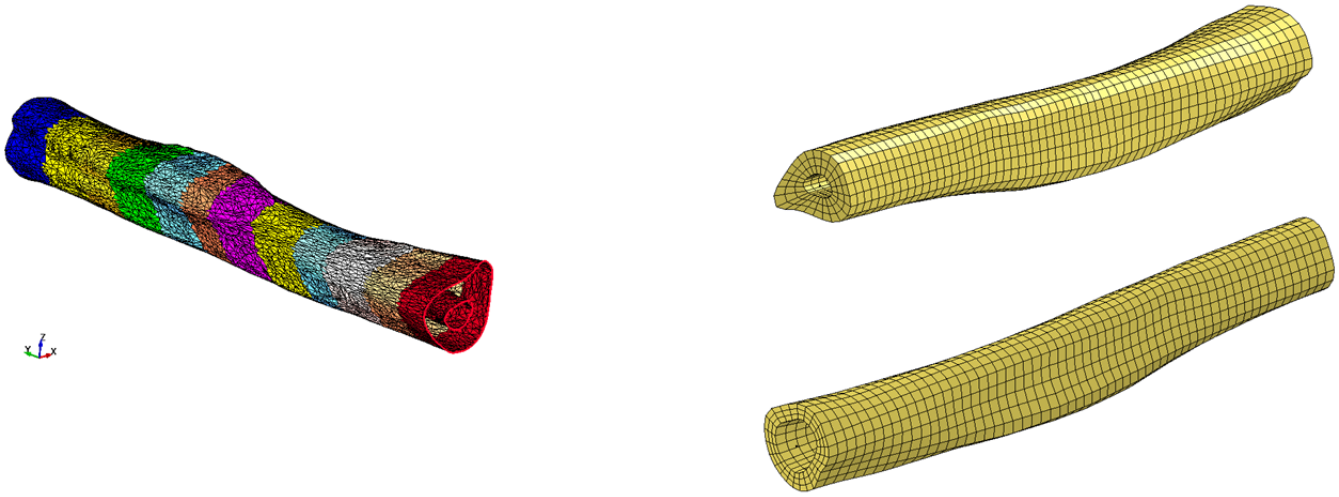

a) Humerus CAD geometry partitioning. b) Humerus FEM mesh using only 4320 hexahedra

Fig. 6. Humerus modeling

The final step in the present investigation was the creation of the global finite element set for the modeling of the low velocity impact of the humerus. For this purpose, two brackets (see Figure 7) have been modeled using Belytschko-Tsay shell elements with the assumption of a rigid elastic material. The whole set of the humerus with the two supports has a total mass of $2453g$, while the mass of the humerus alone (without the two heads) is $135g$. The humerus is connected to the two brackets using rigid link elements, while the center of mass of each rigid bracket is allowed to move along the X-axis and to rotate around the Y-axis as shown in Figure 7.

The impactor of a cylindrical shape with a 20 mm of diameter is modeled using Belytschko-Tsay shell element with the assumption of a rigid elastic material. All contact interfaces are modeled using the CONTACT_SURFACE_TO_SURFACE without friction. The FE simulation is carried out using a total time of 10 ms to cover the entire impact process.

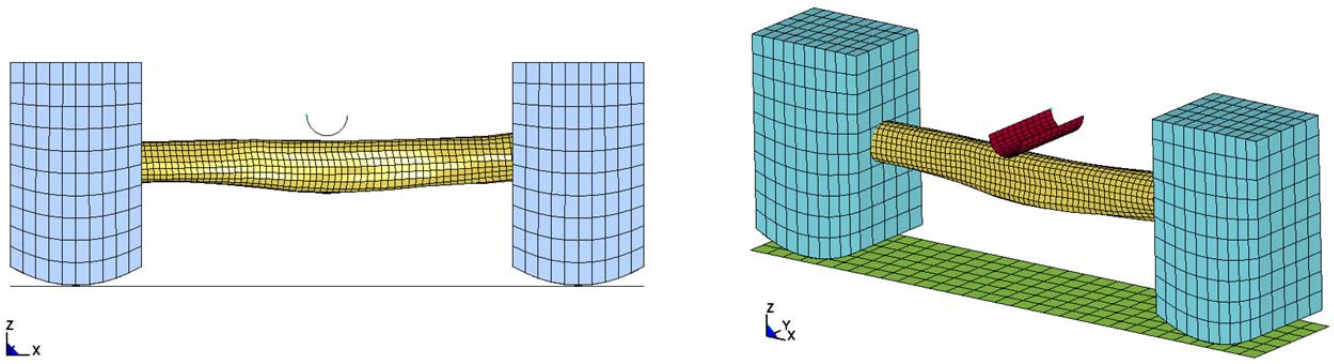

Frontal view Isometric view

Fig. 7. Drop tower modeling using FEM

The total mesh of the whole FEM system includes 4320 hex-shell elements, 1186 Belytschko-Tsay shell elements and 64 rigid link elements. Two concentrated mass elements of 1080*g* for each bracket and a concentrated mass of 6626*g* attached to the impactor taking into account the mass of the cart and the impactor, are considered. For sake of accuracy of the FEM results, no mass scaling is used in the present simulation.
The FE simulation is carried out using the Explicit Dynamic algorithm within LS-DYNA© code, with a total CPU time of *2mn:48s* using a "Dell Precision PWS690" workstation with 2.66*GHz* Intel Xeon processor and 8*GB* of RAM.

III. RESULTS

The experimental campaign of tension/compression on local specimens was conducted as a first attempt to measure the humerus material parameters. The values of humeral bone architectural data are measured for the prismatic-shaped specimens and an estimation of the porosity f_p shows a variation within the range of 1% to 10% which is in concordance with the literature [6]. A set of 46 tests have been done on 5 samples, including 3 in the longitudinal direction of the humerus and 2 in the transverse direction.
A summary of the experimentally measured material parameters is given in Table I. As we can observe from the second column of Table I, all three specimens in longitudinal direction give almost the same estimation of the longitudinal elastic modulus with an average value of $E_l = 21368.33MPa$. The same remark can be done for the two specimens positioned along the transverse direction, with an average value of the transverse elastic modulus of $E_t = 12516MPa$.

TABLE I
SUMMARY OF THE EXPERIMENTALLY MEASURED MATERIAL PARAMETERS

	E_l (MPa)	ν_{lt}	E_t (MPa)	ν_{tl}	d_r (g/mm^3)	f_p
Sample H_1	20619	0.33	–	–	1.992	0.045
Sample H_4	22434	0.37	–	–	1.940	0.084
Sample H_5	21052	0.32	–	–	2.005	0.010
Sample H_2	–	–	12358	0.20	1.962	0.010
Sample H_3	–	–	12674	0.20	1.967	0.011
Average	21368.33	0.34	12516	0.20	1.973	0.032
Standard deviation	773.99	0.02	158	0	0.02	0.02

These experimental results are used to perform the numerical inverse identification of the humerus matrix material parameters.
In the figure 4, the RSM for both longitudinal and transversal moduli identification is presented.

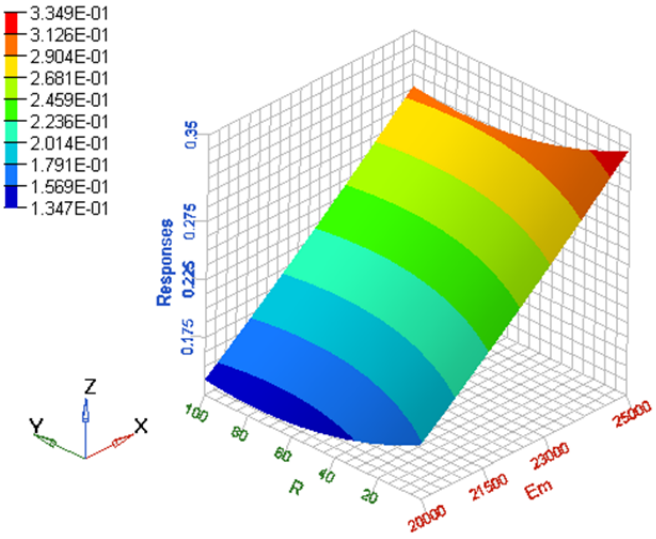

Fig. 4. RSM for both longitudinal and transversal moduli identification

Minimization of the RSM is carried out using a Genetic Algorithm with a mutation rate of 0.01, an elite population percentage of 10%, a discrete states of 1024 and a Random Seed of 1. The minimization procedure gives the results summarized in Table III.

As we can observe on Figure 4, the global minimum has been reached with the optimal matrix elastic modulus $E_m = 20000 MPa$, the maximum allowed porosity of 10% and a void aspect ratio of 75.83 which indicates that the voids shape is closer to a cylindrical cavity rather than a spheroid. We can notice also from the homogenized material parameters (Table IIII) that the obtained elastic moduli in both longitudinal and transverse directions are obtained with approximately the same error compared to the experimental values, with 16% and 13% error respectively.

TABLE III
SUMMARY OF THE NUMERICAL IDENTIFIED MATERIAL (MATRIX AND HOMOGENIZED) PARAMETERS

	E_m (MPa)	ν_m	w	f_p
Matrix properties	20000	0.28	75.83	0.10
	E_l (MPa)	ν_{lt}	E_t (MPa)	ν_{tl}
Homogenized	17997.14	0.28	15200.53	0.28
Measured	21368.33	0.34	12516.00	0.20
Error	0.16		0.13	

As an attempt to study the effects of the elastic moduli in both longitudinal and transverse directions, we conduct a second inverse identification, using only the longitudinal elastic modulus obtained by the three specimens H1, H4 and H5 positioned along the humerus.

The same procedure is applied, and a RSM is built up using a polynomial basis vector of degree 3, where the Analysis of Variance gives an R^2 value of 0.88. Figure 5, shows the RSM for two different porosity values (0 and 5%).

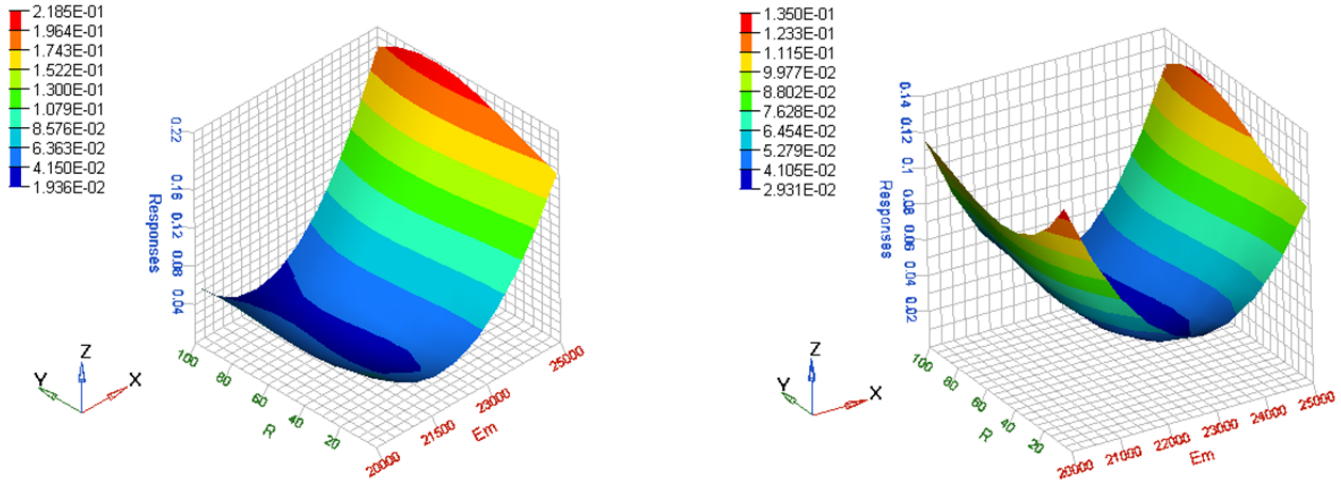

a) RSM with porosity $f = 0$.

b) RSM with porosity $f = 5\%$.

Fig. 5. RSM for longitudinal modulus identification

The minimization procedure in this case gives the results summarized in Table IV. We can see from Figure 5 that the RSM is nonlinear compared to the first RSM. The global minimum is reached with the optimal matrix elastic modulus $E_m = 21606.25 MPa$, absence of porosity (voids) $f_p = 0\%$ and the maximum allowed void aspect ratio of 99.90 which indicates that the voids shape is also of a cylindrical shape along the humerus.

We can notice here, from the homogenized material parameters (Table IV) that the obtained elastic modulus in the longitudinal direction matches exactly the experimental value. As expected, unfortunately in this case the homogenized elastic modulus in the transverse direction is far from the experimentally average value with an error of 40%.

TABLE IV
SUMMARY OF THE NUMERICAL IDENTIFIED MATERIAL PARAMETERS (ONLY E_l IS CONSIDERED)

	E_m (MPa)	ν_m	w	f_p
Matrix properties	21606.25	0.28	99.90	0.00
	E_l (MPa)	ν_{lt}	E_t (MPa)	ν_{tl}
Homogenized properties	21389.97	0.28	21003.24	0.28
Measured properties	21368.33	0.34	12516.00	0.20
Error	0.00		0.40	

Now, we present the result of the FE simulation of the humerus impact. Figure 8 shows the distribution of the impact load history. We can observe globally that a good agreement is obtained for the estimation of the ultimate load between the numerical model and the experimental response.
From Table V, we can notice that both material identification models give approximately the same estimation of the ultimate impact load $2235N$ and $2391N$ with an error of 16.97% and 11.18% respectively.

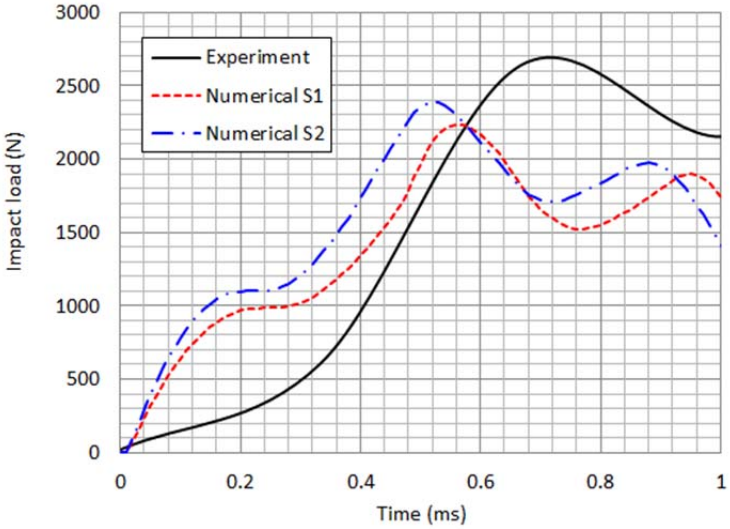

Fig. 8. Impact load (experiment vs numerical)

TABLE V
COMPARISON OF THE ULTIMATE IMPACT LOAD (NUMERICAL VS. EXPERIMENT)

	Time (ms)	Load (N)
Numerical Model 1	0.56	2235
Numerical Model 2	0.52	2391
Experiment	0.71	2692
Error Model 1		16.97%
Error Model 2		11.18%

IV. DISCUSSION

This study is performed to evaluate the ultimate impact load that a human humerus can support. The present study is a first investigation for the mechanical characterization of human humerus using a multi-scale approach. The originality of the proposed procedure consists in the identification of few material parameters to describe a complex anisotropic behavior of the humerus bone. Precisely, only three material parameters are necessary, namely the matrix bone Elastic modulus and two local parameters describing the voids aspect ratio and the porosity to describe the anisotropy.

In the first phase of material identification, using the local specimens with tension/compression tests, we found clearly no significant differences in material parameters between the experimental tests and the proposed multi-scale approach. In fact, both homogenized elastic moduli in longitudinal and transverse directions obtained through the micromechanical model presents only 16% and 17% of error respectively, when compared to the measurements. This indicates the robustness of the proposed multi-scale approach to describe the complex anisotropic behavior of the bone.

Regarding the global validation of the model using a low velocity impact on the humerus, the numerical model under-estimates the ultimate impact load with an error up to 16.97%. This is mainly due to two reasons: first, each of the attached brackets has a big mass which represents eight times the humerus weight and second, the whole set (brackets-humerus) is simply resting on the platform and thus high vibrations may be generated at the impact pulse. Being aware that for these reasons the global humerus response may be blurred to some extent, it becomes difficult to make a concise analysis of the results.

However, despite the aforementioned experimental uncertainties, we remark that the obtained ultimate impact load shows a relatively limited error (16%) compared to the experimental measured load.

Finally, other improvements will be undertaken in the near future to improve these preliminary results. For instance, due to the lack of time, we could not study the friction effects between the brackets and the flat platform, which has probably a non-negligible effect on the global response of the model.

V. CONCLUSIONS

In conclusion, the framework of homogenization is used for the modeling of mechanical behavior for porous bone material. The anisotropic elastic properties of the human humerus are investigated by a coupling between the Mori-Tanaka scheme and experimental measurements of anisotropy using micro-tomography techniques.

The obtained model matches globally the experimental results via the estimation of the ultimate impact load that a human humerus may support before fracture. Further improvements will be made to the present model to be able to simulate the bone fracture by taking into account the nonlinear elastoplastic damage behavior and including the strain rate effects.

VI. ACKNOWLEDGEMENT

The authors are grateful to Rémi Delille and Denis Lesueur, both laboratory engineers at LAMIH, for their valuable help in the preparation of the anatomical specimens and achieving the different scans. Many thanks are also addressed to Pr Xavier Demondion for his earlier work at the laboratory of anatomy of Lille.

VII. REFERENCES

[1] Altair Engineering, HyperMesh© 10.0 User's Guide, Altair Engineering, Inc., World Headquarters: 1820 E. Big Beaver Rd., Troy MI 48083-2031 USA, 2010.

[2] Duprez S, Modélisation en éléments finis du complexe de l'épaule et simulation de sa réponse à un choc latéral, PhD Thesis, Institut National des Sciences Appliquées de Lyon, France, 2007.

[3] Eshelby JD, The determination of the elastic field of an ellipsoidal inclusion, and related problems. Proceedings of the Royal Society Series A, 252, pages 561–569, 1957.

[4] Hannachi M, Naceur H, Batoz JL, Continuum Based Hex-Shell Element Modeling for the Optimization of Composite Multilayered Structures, *International Review of Mechanical Engineering*, vol. 1, issue 4, pages 150–163, 2007.

[5] Hill R., A self-consistent mechanics of composite materials, *Journal of the Mechanics and Physics of Solids*, vol. 13, pages 213–222, 1965.

[6] Laval-Jeantet A-M, Bergot C, Carroll R, Garcia-Schaefer F, Cortical Bone Senescence and Mineral Bone Density of the Humerus, *Calcified Tissue International*, Vol. 35, pages 268–272, 1983.

[7] LS-DYNA© Keyword User's Manual, Version 971, Livermore Software Technology Corporation (LSTC), May 2007.

[8] Ma XQ, Morphological effects of mechanical forces on the human humerus, *British Journal of Sports Medicine*, Vol. 26, issue 1, pages 51–53, 1992.

[9] Mori T, Tanaka K, Averages stress in matrix and average elastic energy of materials with misfitting

inclusions, *Acta Metallia*, vol. 21, pages 571–574, 1973.

[10] Rahmoun J, Chaari F, Markiewicz E, Drazetic P, Micromechanical modeling of theanisotropy of elastic biological composites, *Multiscale Modeling and Simulation*, vol. 8, n^o 1, pages 326-336, 2009.

[11] Satoru Saitoh MD, Yuklo Nakatsuchi MD, Osteoporosis of the proximal humerus: Comparison of bonemineral density and mechanical strength with the proximal femur, *Journal of Shoulder and Elbow Surgery*, vol. 2, pages 78–84, 1993.

[12] Schoenfeld CM, Lautenschlager EP, Meyer Jr PR, Mechanical properties of human cancellous bone in the femoral head, *Medical and Biological engineering,* vol. 12, pages 313–317, 1974.